



# Interfacial supercooling and the precipitation of hydrohalite in frozen NaCl solutions as seen by X-ray absorption spectroscopy

Thorsten Bartels-Rausch<sup>1</sup>, Xiangrui Kong<sup>1,a</sup>, Fabrizio Orlando<sup>1,b</sup>, Luca Artiglia<sup>1</sup>, Astrid Waldner<sup>1</sup>, Thomas Huthwelker<sup>2</sup>, and Markus Ammann<sup>1</sup>

<sup>1</sup>Laboratory of Environmental Chemistry, Paul Scherrer Institut, Villigen PSI, Switzerland

<sup>2</sup>Swiss Light Source (SLS), Paul Scherrer Institut, Villigen PSI, Switzerland

<sup>a</sup>now at: Department of Chemistry and Molecular Biology, Atmospheric Science, University of Gothenburg, Gothenburg, Sweden

<sup>b</sup>now at: Omya International AG, Oftringen, Switzerland

**Correspondence:** Thorsten Bartels-Rausch (thorsten.bartels-rausch@psi.ch)

Received: 1 September 2020 – Discussion started: 27 November 2020

Revised: 3 March 2021 – Accepted: 4 March 2021 – Published: 23 April 2021

**Abstract.** Laboratory experiments are presented on the phase change at the surface of sodium chloride–water mixtures at temperatures between 259 and 241 K. Chloride is a ubiquitous component of polar coastal surface snow. The chloride embedded in snow is involved in reactions that modify the chemical composition of snow as well as ultimately impact the budget of trace gases and the oxidative capacity of the overlying atmosphere. Multiphase reactions at the snow–air interface have been of particular interest in atmospheric science. Undoubtedly, chemical reactions proceed faster in liquids than in solids; but it is currently unclear when such phase changes occur at the interface of snow with air. In the experiments reported here, a high selectivity to the upper few nanometres of the frozen solution–air interface is achieved by using electron yield near-edge X-ray absorption fine-structure (NEXAFS) spectroscopy. We find that sodium chloride at the interface of frozen solutions, which mimic sea-salt deposits in snow, remains as supercooled liquid down to 241 K. At this temperature, hydrohalite exclusively precipitates and anhydrous sodium chloride is not detected. In this work, we present the first NEXAFS spectrum of hydrohalite. The hydrohalite is found to be stable while increasing the temperature towards the eutectic temperature of 252 K. Taken together, this study reveals no differences in the phase changes of sodium chloride at the interface as compared to the bulk. That sodium chloride remains liquid at the interface upon cooling down to 241 K, which spans the most common temperature range in Arctic marine environments,

has consequences for interfacial chemistry involving chlorine as well as for any other reactant for which the sodium chloride provides a liquid reservoir at the interface of environmental snow. Implications for the role of surface snow in atmospheric chemistry are discussed.

## 1 Introduction

Chemical cycling of halogens affects the composition of the troposphere and via this effect influences climate and impacts human health (Simpson et al., 2007; Abbatt et al., 2012; Saiz-Lopez and von Glasow, 2012; Simpson et al., 2015). Given the abundance of chloride in the form of sea salt over wide areas of the globe, the atmospheric chemistry of chlorine has long raised interest in several multiphase reactions that liberate chloride into chlorine species in the gas phase (Simpson et al., 2007; Finlayson-Pitts, 2010). Chlorine has a direct role as a sink for ozone. Further, reactive chlorine species act as a powerful oxidant on atmospheric cycles that destroy or produce ozone and are relevant for the atmospheric oxidation capacity (Finlayson-Pitts, 2003; Thornton et al., 2010). Atmospheric ozone is of concern because it directly impacts atmospheric composition, health, and climate (Simpson et al., 2007). Prominent examples of these reactions in the atmosphere with chloride in sea salt or salt dust are shown in Fig. 1 and discussed in the following. Acid displacements, where nitric or sulfuric acid is taken up into the aqueous phase,

lead to the emission of hydrochloric acid to the gas phase. Further examples are reactions with OH radicals (Knipping et al., 2000; Halfacre et al., 2019) and with nitrogen oxides (Osthoff et al., 2008). Common to all of these reactions is the generation of chlorine gases that either react with OH radicals or photolyse at wavelengths available in the troposphere to generate reactive chlorine (Fig. 1 and Finlayson-Pitts, 2010). Given their importance, these multiphase reactions have been intensively investigated in laboratory studies over the last decade (Abbatt et al., 2012; Saiz-Lopez and von Glasow, 2012; Simpson et al., 2015). One outcome of these investigations is the importance of reactions at the liquid–air interface as compared to those proceeding in the bulk. An example is the oxidation of chloride by OH radicals. In contrast to the aqueous-phase reactions, it does not require the presence of acid to proceed fast at the air–water interface (Laskin et al., 2006).

The relevance of halogen multiphase chemistry for the atmosphere is not limited to chlorine. A more recent example is the oxidation of bromide. Bromide is present in sea salt, is a key reactant in ozone depletions in polar atmospheres (Simpson et al., 2015), and participates in atmospheric chlorine chemistry by forming interhalogen compounds (Finlayson-Pitts, 2003). Oldridge and Abbatt (2011) have shown that a Langmuir–Hinshelwood type surface reaction of ozone with bromide occurs at the liquid–air interface simultaneously with a corresponding bulk reaction in the temperature range of 263 to 248 K. A surface-active reaction intermediate was found to explain the high interfacial reactivity for the case of the reaction with ozone (Artiglia et al., 2017), while other bromine species may directly exhibit surface propensity on their own (Gladich et al., 2020). Clearly, this line of research shows how reaction kinetics and mechanisms differ at the interface from those in the bulk and that heterogeneous chemistry is a key driver in atmospheric chemistry.

In the cryosphere, where the snowpack strongly impacts the chemistry in the overlaying atmosphere (Dominé and Shepson, 2002; Thomas et al., 2019), halogen compounds are also found within the snow. Sea-salt components, a source of halogens in snow in coastal snowpack, might originate from migration from underlying sea ice or from deposition of wind-transported sea-spray aerosols (Dominé et al., 2004). One characteristic of the cryosphere is its subfreezing temperatures and the consequent precipitation of chemical constituents at a specific temperature, their eutectic temperature, as also observed in sea ice (Petrich and Eicken, 2009). It is known that the precipitations or phase changes of the reactants critically impact the reactivity (Bartels-Rausch et al., 2014; Kahan et al., 2014). Reduced chlorine production in frozen systems was observed by Wren et al. (2013) and by Sjøstedt and Abbatt (2008), at temperatures below the eutectic temperature of sodium chloride–water mixtures in laboratory experiments that was attributed to the precipitation of the salt. In an Arctic field study, Custard et al. (2017) observed reduced  $\text{Cl}_2$  production when temperatures dropped and sug-

gested limited availability of chloride as a consequence of the precipitation in this surface snow. Further, Lopez-Hilfiker and Thornton (2012) proposed the precipitation of sodium chloride salts to explain the changes in the production yield of  $\text{ClNO}_2$  from the reaction of  $\text{N}_2\text{O}_5$  with saline frozen systems with temperature.

More generally, it is not only the chlorine chemistry that responds to the phase of sodium chloride present in frozen systems both in the laboratory and in the environment. Oldridge and Abbatt (2011) showed that the rate of the heterogeneous reaction of ozone with bromide in sodium chloride–water mixtures is strongly reduced once the chloride salt precipitates below 252 K. The authors explained this with the reduction in liquid volume that serves as a reaction medium for the bromide in the sample due to the precipitation of sodium chloride. Similarly, the photolytical reaction of nitroanisole with pyridine was found to depend on the amount of liquid in frozen samples and thus to critically respond to precipitation of sodium chloride (Grannas et al., 2007). Next to its role in atmospheric halogen chemistry, sodium chloride is thus of further importance as salt to establish and maintain liquid solutions at subfreezing temperatures. Its importance arises from its atmospheric abundance but also because its eutectic temperature of 252 K corresponds to typical springtime Arctic temperatures – a region and time period where atmospheric halogen chemistry is most active. For example, at the Arctic coast near Utqiagvik (Alaska) temperatures have been reported to fluctuate between 247 K and 259 K within days (Custard et al., 2017). Another region of Earth's cryosphere, where temperatures drop below 252 K, is the troposphere (Thomas et al., 2019). Wang et al. (2015) have proposed a significant role of tropospheric heterogeneous halogen chemistry on the ozone budget there. More recently, Murphy et al. (2019) have shown that the quantity of sea-salt aerosols lifted to the upper troposphere is small, casting some doubt on the environmental relevance of sea salt as a matrix for multiphase chemistry there.

While the phase diagram of sodium chloride–water binary mixtures and the thermodynamic stability domains of salt, solution, and ice are well known (Koop et al., 2000a), the precise occurrence of nucleation and sodium chloride precipitation is still debated (Koop et al., 2000a; Wise et al., 2012; Peckhaus et al., 2016). Figure 2 shows a part of the phase diagram of sodium chloride–water mixtures and can be used to illustrate the appearance of the individual phases. Below 251.9 K, the eutectic temperatures of sodium chloride (Koop et al., 2000a), solid sodium chloride dihydrate (hydrohalite,  $\text{NaCl}\cdot 2\text{H}_2\text{O}$ ), and solid water (ice) are the energetically favoured phases. Between the eutectic temperature and the so-called liquidus line, ice and sodium chloride solutions (brine) co-exist. The ice will melt completely above the liquidus line, and an aqueous sodium chloride solution is the only phase present. The focus of this work was to experimentally observe phase changes of sodium chloride be-

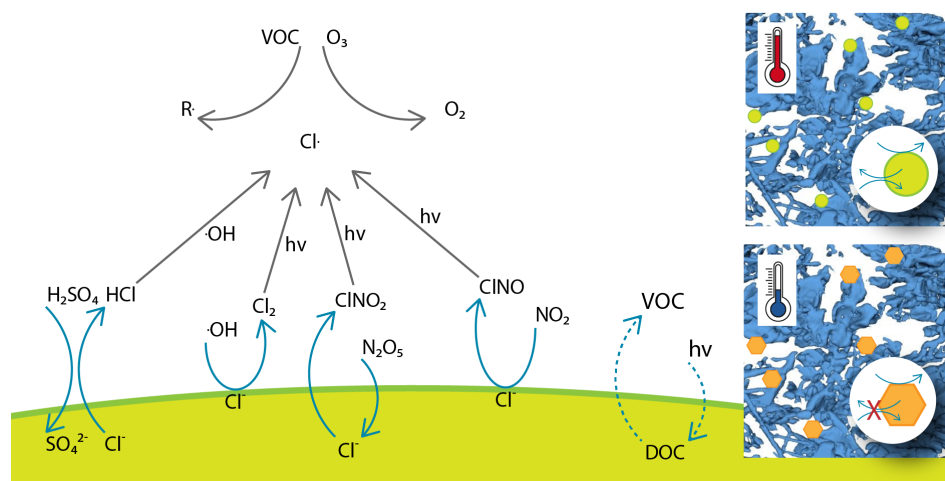


**Figure 1.** Simplified scheme of multiphase reactions liberating chlorine from sea-salt deposits to the atmosphere and subsequent reactions of chlorine with impacts on the ozone budget and air quality. These reactions may occur both in the bulk phase and at the air–deposit interface for liquid particles. The sea salt may also maintain a liquid phase for the reaction of other reactants such as the photolysis of organics. The inserts illustrate sea-salt deposits in snow and how phase changes from solid (orange hexagon) to aqueous solutions (green circle) impact the chemical reactivity. See text for details and references.

low the eutectic temperature. A typical experimental procedure started with a dry sample of anhydrous sodium chloride (halite, NaCl) which was exposed to increasing gas-phase water at a constant temperature of 259 K. By absorbing water from the surrounding air, a phase transition from the solid salt to a liquid solution (deliquescence) took place. Upon increasing the gas-phase water dosing further (Fig. 2, red arrow), ice crystallized and a two-phase system of ice and brine occurred (Fig. 2, red cross). After probing the sample at this position in the phase diagram, temperature was lowered and the dosing of the water vapour was adopted to move along the liquidus line to below the eutectic temperature. During this cooling period, salt concentration and volume of the brine changes. Such changes with varying relative humidity (hygroscopic growth) have long been discussed for aerosols in the troposphere. In other words, the concentration of the sodium chloride in solution changes with temperature to maintain both phases in equilibrium. At the air–ice interface where both phases are in equilibrium with water vapour in the gas phase, this can be understood by considering that the aqueous sodium chloride solution and ice need to have the same vapour pressure. Otherwise, the phase with the higher water vapour pressure would vanish by evaporation and the one with the lower vapour pressure would grow by condensation. The vapour pressure of ice decreases with decreasing temperature, while that of an aqueous solution decreases with increasing concentration of solute. With a fixed amount of sodium chloride present in our experiments and also in individual sodium chloride deposits in snow, the amount of liquid is consequently given by temperature (Koop et al., 2000a). Because relative humidity is such a strong driver of the hygroscopic growth, we base the discussion of phase changes in

this work on the relative humidity the sample was exposed to. The relative humidity is a measure of the partial pressure of water relative to the vapour pressure of (supercooled) liquid at the same temperature (Marti and Mauersberger, 1993). An advantage of this experimental approach with environmental relevance is that the relative humidity precisely matches that in the atmosphere in contact and in thermodynamic equilibrium with ice clouds or snow cover, because the relative humidity is a sole function of temperature in the presence of ice. Therefore, the chemical concentration of such particles exactly matches those of the same composition in snow or in the atmosphere under environmental conditions.

Koop et al. (2000a) were the first to show that because precipitation of sodium chloride can be kinetically hindered, supercooled sodium chloride solutions in the presence of ice can prevail down to 240 K. Precipitation of sodium chloride may not occur even though temperature has dropped below the eutectic temperature where the solid is the thermodynamically favoured phase. Cho et al. (2002) have observed a liquid fraction in sodium chloride–water mixtures at even lower temperatures of between 228 and 273 K based on the evaluation of  $^1\text{H-NMR}$  signals. Cho et al. (2002) proposed the presence of liquid below the eutectic temperature to be an interfacial phenomenon, stabilized by surface forces in analogy to the disordered interface observed for neat ice surfaces when approaching the melting point (Bartels-Rausch et al., 2014).

The goal of this study is to investigate the precipitation and the occurrence of liquid features in sodium chloride–water binary mixtures in the interfacial region. Both Cho et al. (2002) and Koop et al. (2000a) have applied methods that are not specifically sensitive to the interface but probe the

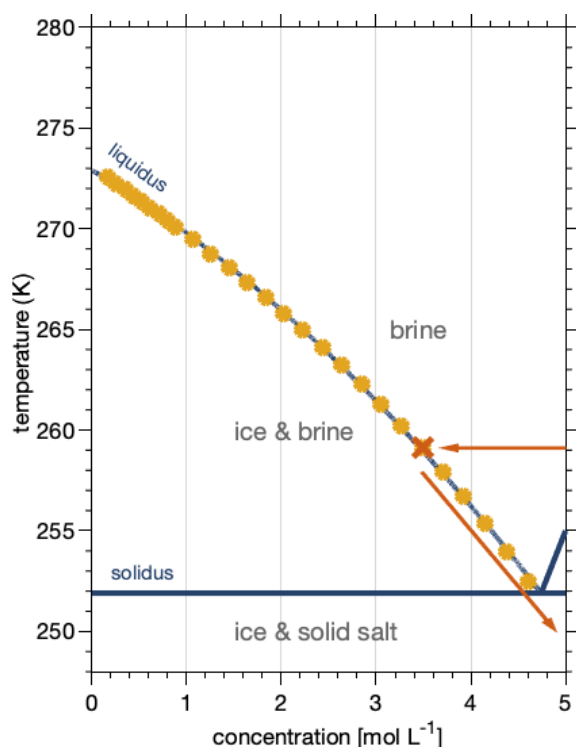


**Figure 2.** Phase diagram of the sodium chloride–water binary system. The data show the freezing-point depression of sodium chloride solutions (filled yellow circles) and give the concentration of an aqueous sodium chloride solution in equilibrium with ice in the temperature range of 273 to 254 K (Rumble, 2019). The dark-blue lines indicate the phase boundaries (Koop et al., 2000b; Rumble, 2019); that is they denote the so-called liquidus and solidus line, respectively, and thus show the temperature and concentration range where ice and aqueous sodium chloride solutions co-exist. The eutectic temperature of sodium chloride–water binaries is 251.9 K (Koop et al., 2000a). Also shown is a typical experimental procedure (red arrows and cross).

bulk. Near-edge X-ray absorption fine-structure (NEXAFS) spectroscopy is inherently sensitive to the upper few nanometres of interfaces when detecting electrons as performed in this work. Oxygen K-edge NEXAFS spectra of H<sub>2</sub>O are an established tool to investigate the hydrogen-bonding structure of water and ice with its clear differences for solid and liquid water (Bluhm et al., 2002; Nilsson et al., 2010; Krepelova et al., 2013; Newberg and Bluhm, 2015; Orlando et al., 2016; Bartels-Rausch et al., 2017; Ammann et al., 2018; Waldner et al., 2018). In our earlier NEXAFS study (Krepelova et al., 2010a), it was shown by probing the X-ray absorption of oxygen atoms in sodium chloride–water binary mixtures that the hydrogen-bonding network did not reveal the presence of any liquid features at the interface below the eutectic temperature. Interpretation of these oxygen NEXAFS spectra was complicated by the appearance of crystal water in the hydrohalite and by the presence of adsorbed H<sub>2</sub>O. Also, the oxygen spectra might be dominated by ice

that is present in equilibrium with the sodium chloride solution, and thus small fractions of liquid might have been difficult to detect. In this work, we therefore discuss Cl K-edge NEXAFS that has previously been used to inspect the chemical speciation of chlorine in glasses and in coal (Huggins and Huffman, 1995; Evans et al., 2008). Interest in the local environment of chloride at the interface in sodium chloride–water binary mixtures also comes from earlier work on nitric and hydrochloric acid adsorbed at the ice–air interface. We have shown that nitrate and chloride form solvation shells with a hydrogen-bonding structure similar to that in aqueous solutions in the interfacial region of ice at concentrations low enough to prevent melting (Krepelova et al., 2010b; Kong et al., 2017). The aim of this study is thus also to investigate the occurrence of solvated chloride at the interface of sodium chloride–water mixtures at temperatures close to the eutectic one. Motivation comes from the role of heterogeneous chemistry in atmospheric science in general and in particular on the impact that the microchemical environment has on the reactivity.

## 2 Experimental part

Experiments were performed at the PHOENIX beamline of the Swiss Light Source (SLS) at the Paul Scherrer Institute using the near-ambient pressure photoemission (NAPP) set-up previously described (Orlando et al., 2016). NAPP is equipped with a differentially pumped electron analyser (Scienta R4000 HiPP-2). The central feature of NAPP is a flow-through cell with a sample holder, the temperature of which is computer-controlled by a flow of cooled helium gas. The measurements were performed with partial pressures of water between 0.3 and 1.8 mbar in the flow-through cell and temperatures of the sample between 259 and 241 K.

### 2.1 Sample preparation and water dosing

To prepare a sample, 1  $\mu$ L of a 2.12 g sodium chloride (Fluka TraceSELECT 38979-25G-F) solution in 80 mL of water (Fluka TraceSELECT 142100-12-F) was dropped at the centre of the sample holder and dried at 60 °C. The sample holder was then moved into the flow-through cell and kept at ultra-high vacuum and at 60 to 80 °C for 45 min to remove volatile impurities. Water vapour was dosed to the flow-through cell via a 0.8 mm i.d. steel capillary from the vapour above liquid water (Fluka TraceSELECT 142100-12-F) in a vacuum-sealed, temperature-controlled glass reservoir. Before dosing, the water was degassed by four freeze-pump–thaw cycles. The water dosing and thus the partial pressure or relative humidity that the sample were exposed to was varied by setting the temperature of the reservoir to change the flux of water vapour into the experimental cell. Pressure in the flow-through cell was monitored by a capacitance manometer (Baratron 626A) with a measurement

range from  $5 \times 10^{-4}$  to 10 mbar and an accuracy of 0.25 % of the reading. Temperature was monitored with a Pt1000 sensor located at the edge of the sample holder. The sensor was calibrated prior to the experiments by growing ice on the sample holder and noting its vapour pressure which is a direct measure of the temperature at the sample spot (Marti and Mauersberger, 1993). During the experiments, the calibration was confirmed when ice was present. At 253 K, the offset between the temperature reading and calibration was found to be  $4.3 \pm 0.2$  K.

## 2.2 X-ray-excited electron spectroscopy

Partial Auger–Meitner electron yield NEXAFS spectra at the Cl K-edge were acquired with a fixed kinetic-energy window of 2370 to 2390 eV, which includes the KL<sub>2,3</sub>L<sub>2,3</sub> Auger–Meitner peak of chlorine. The pass energy and dwell time were set to 200 eV and 300 ms, respectively. The distance of the sample to the electron analyser inlet (working distance) was 1 mm. The electron analyser was operated with an electron sampling aperture with a diameter of 500  $\mu$ m, which results in sampling roughly an area on the icy sample with a diameter of 500  $\mu$ m from which the emitted electrons reach the detector. NEXAFS spectra were measured by sweeping the incident X-ray photon energy across the chlorine K-edge from 2815 to 2845 eV with steps ranging from 0.2 to 1 eV. The NEXAFS spectra were processed by dividing by the photon flux ( $I_0$ ) as derived in situ using a Ni-coated membrane, subtracting the mean pre-edge intensity as background, and normalizing to the mean intensity at 2830 to 2833 eV X-ray photon energy. Photoemission spectroscopy (XPS) spectra of O1s, Cl2p, Na1s, C1s, and Au4f were recorded at an incident X-ray photon energy of 2200 eV and with a pass energy of 100 eV and a dwell time of 120 ms. To quantify, a linear background was applied, and the photoemission signal was integrated in MATLAB without any peak fitting.

## 3 Results and discussion

### 3.1 NEXAFS of brine, halite, and hydrohalite

Figure 3 shows chlorine K-edge X-ray absorption spectra of sodium chloride salts and of frozen NaCl–water binary mixtures in the presence of ice. This NEXAFS spectroscopy probes the X-ray absorption by chlorine atoms, corresponding to the resonant excitation of core electrons into unoccupied molecular orbitals. As exactly those outer orbitals are forming chemical bonds, NEXAFS spectra directly reflect changes to the local chemical environment and structural arrangement. NEXAFS spectroscopy of halogen salts has thus been used to discuss their phase and chemical speciation in geological examples (Huggins and Huffman, 1995; Evans et al., 2008). In this work, the X-ray absorption spectra were derived by recording the intensity of Auger–Meitner elec-

trons at 2370–2390 eV, which corresponds to the KL<sub>2,3</sub>L<sub>2,3</sub> transition in chlorine (Cleff and Mehlhorn, 1969). Detecting electrons, as carried out in this work, makes X-ray absorption inherently surface sensitive, because electrons have a limited escape depth in matter (Ammann et al., 2018). The escape depth can be quantified by relating it to the inelastic mean free path (IMFP) of electrons in matter and to the take-off angle of detected electrons relative to the surface normal. The IMFP of electrons with a kinetic energy of 2380 eV is about 7 nm in NaCl and in ice (Tanuma et al., 1991). The take-off angle of electron detection is 30° in our set-up (Orlando et al., 2016), which gives an escape depth of 6 nm, meaning that cumulatively, 95 % of the electrons detected originate from 18 nm, with an exponentially decreasing contribution from the surface towards the bulk. In the following, we report the NEXAFS spectra derived from this interfacial region of NaCl–water binary mixtures to discuss changes in the solvation of chloride by water as we explore the regions of the phase diagram where precipitation of sodium chloride has been described for bulk samples.

All chlorine K-edge spectra show a strong absorption peak at 2825–2830 eV (region I), the absorption edge, corresponding to the transition of electrons from the 1s orbital to the empty 4p orbitals. Halite salt, in Fig. 3a, shows a strong absorption in region I and a characteristic feature at 2838 eV (region II) (Huggins and Huffman, 1995; Evans et al., 2008). The difference in the relative intensity of region I as compared to the intensity at photon energies > 2830 eV between Fig. 3a and Huggins and Huffmann (1995) comes from the latter using fluorescence as a detection mode. Detecting X-ray absorption with fluorescence probes deeper into the bulk of the samples and therefore often suffers from self-absorption which leads to fewer signal intensities at the absorption edge (region I).

The small feature at 2821 eV can be assigned to C–Cl bonds that may form in situ due to reactions involving secondary electrons and organic impurities (Fujimori et al., 2010). The sample composition in the interfacial region was further investigated by X-ray photoemission spectroscopy. The C1s and Cl2p spectra support the presence of C–Cl compounds in the samples (Appendix A): a small feature in the Cl2p spectra at a binding energy 3 eV higher than the main chlorine signal might be attributed to organic carbon species. The C1s photoemission spectra show a feature at a binding energy 1.5 eV higher than the main feature, typical of C–Cl compounds. The main feature of the C1s photoemission spectra is attributed to C–H bonds, the dominant component of adventitious carbon that forms in a cascade of reactions with secondary electrons during the experiments. A further source of carbon might be omnipresent traces of carbon in the NaCl and introduced when preparing the NaCl samples. The atomic ratio of the total carbon to oxygen from water present at the interface was below 0.25, except for samples in Fig. 3a and f where total carbon-to-oxygen atomic ratios were 0.5–0.75. Adsorbed water molecules were present at the interface

of all samples, and ice or liquid water formed in some samples, as gaseous water was present in all experiments with pressures between 0.3 and 1.8 mbar. The atomic ratio was derived based on the measured Cl1s/O1s photoemission intensities and a calibration to account for the analyser efficiency and total X-ray photoionization cross section using Cl1s/O1s photoemission intensities of 0.8 mbar CO<sub>2</sub> gas following a procedure used before (Krepelova et al., 2013). Direct comparison between the individual samples and estimation of surface coverages of the carbon impurities is hampered by the varying water content at the sample's interface as adsorption and water uptake varies with the individual relative humidity settings.

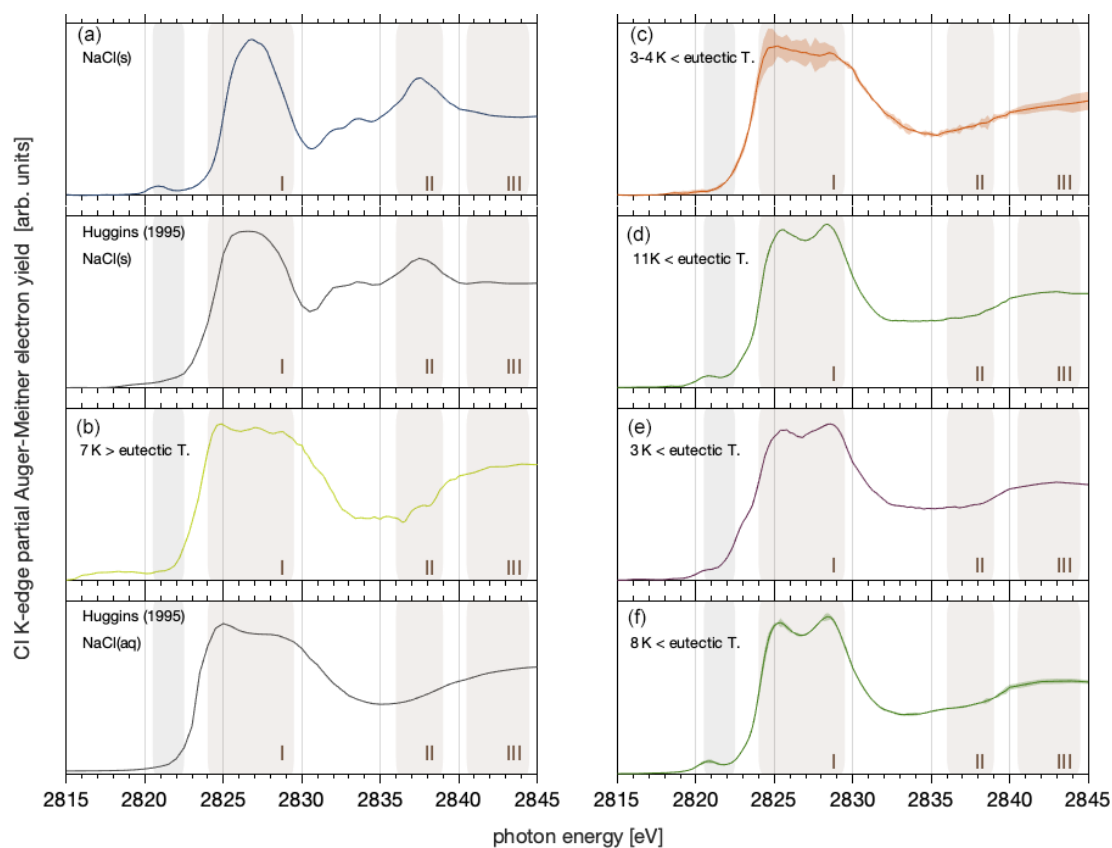
The spectrum of sodium chloride in aqueous solutions, Fig. 3b, shows a broader absorption peak in region I compared to the spectra of the halite and a second feature at 2840 eV (region III) (Huggins and Huffman, 1995). In this work, the NEXAFS spectrum of NaCl in aqueous solutions was recorded in a solution–ice binary mixture based on the phase diagram (see Sect. 3.2, “Efflorescence at the interface”). Based on freezing-point depression data, the concentration of sodium chloride in such an aqueous solution in equilibrium with ice is 3.5 mol L<sup>-1</sup> (Rumble, 2019). The spectrum in Fig. 3b generally agrees with the X-ray absorption spectra reported for 0.1 and 1 mol L<sup>-1</sup> aqueous solutions (Huggins and Huffman, 1995) as it captures the general decrease in intensity in region I with excitation energy and the increase in absorption in region III (Fig. 3). Discussing differences in the hydration structure of chloride at the water–air interface as compared to the bulk solution is beyond the scope of this work. Harada et al. (2011) have reported differences in the hydration structure of Br<sup>-</sup> at the aqueous surface compared to in bulk. Due to the low spectrum quality, evident by the wiggles in region I, we refrain from discussing the two distinct features in region I, at 2824 and 2829 eV, that have been observed in previous work on NEXAFS spectra of aqueous chloride solutions (Huggins and Huffman, 1995; Antalek et al., 2016).

Figure 3c–e show NEXAFS spectra acquired in the ice stability domain at temperatures below the eutectic temperature of 251.9 K (Koop et al., 2000a). By comparing these spectra to the spectra in Fig. 3a and b, the phase of the sodium chloride in the presence of ice below the eutectic temperature will be discussed. When cooling to 248–249 K from above the eutectic temperature, the NEXAFS spectrum resembles that of a typical aqueous solution (Fig. 3c). Figure 3c shows an average of three individual NEXAFS spectra which still show substantial scatter that results in a low spectra quality. We assign the spectral quality to the low amount of salt within the interfacial region and to potential thermal circulations and thus redistribution of the liquid during the measurements upon irradiation by the beam. Despite this uncertainty, the results in Fig. 3a–c allow us to clearly differentiate between solid halite and aqueous solutions.

Upon cooling further to 241 K, the spectrum changed significantly. The NEXAFS spectrum in Fig. 3d shows a wide peak in region I with two well-resolved features about 3 eV apart. That both features have a similar intensity makes this spectrum clearly distinct from those of an aqueous NaCl solution with its decreasing trend of absorption in region I. Compared to the spectrum of aqueous NaCl solutions (Fig. 3b, c), the absorption edge is shifted to higher photon energies in the spectrum in Fig. 3d. The absence of a feature in region II makes the spectrum in Fig. 3d distinct from the spectrum of anhydrous NaCl salt. Notably, the spectrum quality is greatly improved and is similar to that of the solid, anhydrous halite sample (Fig. 3a). One factor impacting the spectral quality is the stability of the sample during the NEXAFS acquisition. The analysis of the Cl2p photoemission spectra acquired before and after each NEXAFS run showed that the amount of chlorine detected in the sample volume fluctuated by less than 10 %, between 0 % and 9 %, in samples shown in Fig. 3c–f (Appendix A). For comparison, samples in Fig. 3a and b showed a decrease of 39 % and 43 % in the integrated Cl2p signal intensity from prior to to after, respectively, the NEXAFS was recorded. Possible reasons for these trends are an increase in adsorbed water with time masking the intensity of the underlying chlorine (Fig. 3a) and changes in the distance of the sample to the electron analyser with time leading to a reduction in the intensities of all compounds (Fig. 3b). Both processes would also affect the NEXAFS signal by inducing changes in intensity with time. Direct quantitative comparison is beyond the scope of this work and is hampered by the different probing depths of XPS and NEXAFS as given by the kinetic energy.

We assign the spectrum in Fig. 3d to that of sodium chloride dihydrate (hydrohalite, NaCl·2H<sub>2</sub>O). The NEXAFS spectrum of the hydrohalite has to the best of our knowledge not been described before. The double-peak feature in region I, which we observe in this work, is typical of other chloride hydrates such as MnCl<sub>2</sub>·4H<sub>2</sub>O, CaCl<sub>2</sub>·2H<sub>2</sub>O, and MgCl<sub>2</sub>·6H<sub>2</sub>O (Evans et al., 2008). It is also present in the NEXAFS spectra of sodium chloride solutions (Huggins and Huffman, 1995), with a different ratio of the two features as observed here for the hydrohalite. Antalek et al. (2016) have explained this double-peak feature in NEXAFS spectra of aqueous chloride solutions by the formation of two distinct solvation shells with two distances between the chloride and the solvating water molecules based on NEXAFS and extended X-ray absorption fine-structure spectroscopy as well as molecular dynamics simulations. We propose here that the NEXAFS spectra of the hydrohalite can be understood based on the same argument, as the chloride in NaCl·2H<sub>2</sub>O is coordinated by two sodium and four water molecules with two distinct distances of Cl to the neighbouring oxygen of the water molecules (Klewe et al., 1974).

Figure 3e shows a spectrum after warming the sample back to 249 K in the presence of ice. Clearly, the observed shape in region I shows that hydrohalite and not liquid brine is the



**Figure 3.** Partial electron yield chlorine K-edge NEXAFS spectra of the sodium chloride–water binary system: **(a)** Sample A – solid NaCl at 248 K and 44 % relative humidity (0.34 mbar water vapour pressure). **(b)** Sample B – Aqueous NaCl solution in equilibrium with ice at 88 % RH (1.82 mbar) and 259 K. **(c)** Sample C – an averaged spectrum at the thermodynamic ice stability line at 248 K to 249 K and 78 % (0.60 mbar) to 80 % (0.71 mbar) RH. **(d)** Sample D – an individual spectrum upon further cooling to 241 K and 74 % RH (0.29 mbar). **(e)** Sample E – an individual spectrum upon heating back to 249 K in the ice stability domain at 79 % RH (0.69 mbar). **(f)** Sample F – the averaged spectrum at 244 K and a RH of 59 % (0.32 mbar) and 73 % (0.40 mbar), lower than the ice stability domain. See Fig. 4 for precise measurement settings. The shaded coloured areas of the graphs in **(c)** and **(f)** denote the standard deviation of three and two repeated NEXAFS acquisitions. Also shown for comparison are NEXAFS spectra of NaCl salt and aqueous solutions that were detected in a fluorescence mode and not via partial electron yield (Huggins and Huffman, 1995, denoted as Huggins (1995) in the figure). The brownish shaded area (I–III) highlights regions in the NEXAFS spectra discussed in the text. The grey-shaded area at 2821 eV highlights the photon energy region where carbon–chlorine bonds from carbon contamination might show an absorption feature (see text for details).

dominant phase of this sample. In Fig. 3f an averaged spectrum at 244 K in the absence of ice is shown; again the shape is in good agreement with the spectrum shown in Fig. 3d. We would like to note the excellent reproducibility of the spectra as seen in Fig. 3f by the small standard deviation of two samples (shaded area). In summary, we have clearly presented three different chlorine K-edge NEXAFS spectra and argued that these derive from the halite, chloride solution, and hydrohalite. Hydrohalite at the air–ice interfacial region was thus observed in the temperature range 241–249 K.

### 3.2 Efflorescence at the interface

Now that we have identified halite, the hydrohalite, and chloride in an aqueous solution by means of the NEXAFS spectra at the interfacial region, we discuss their observation in the

phase diagram. Generally, we have observed solid sodium chloride as halite or hydrohalite in the temperature range of 241 to 249 K and at 44 % to 79 % RH and as brine in the temperature range of 248 to 259 K and RH of 78 %–88 %.

Interestingly, the NEXAFS spectra have revealed the dominant presence of brine in one sample and of hydrohalite in other samples below the eutectic temperature. This clearly shows that not only the temperature and relative humidity but also the trajectory to reach these settings (or the history of the sample) determine the phase. Therefore, we will detail the humidity and temperature history of each sample in the following. Also, we will compare our findings to the extensive literature work of observed phases in the presence and absence of ice. This discussion will be based on the sodium chloride–water phase diagram in the temperature–

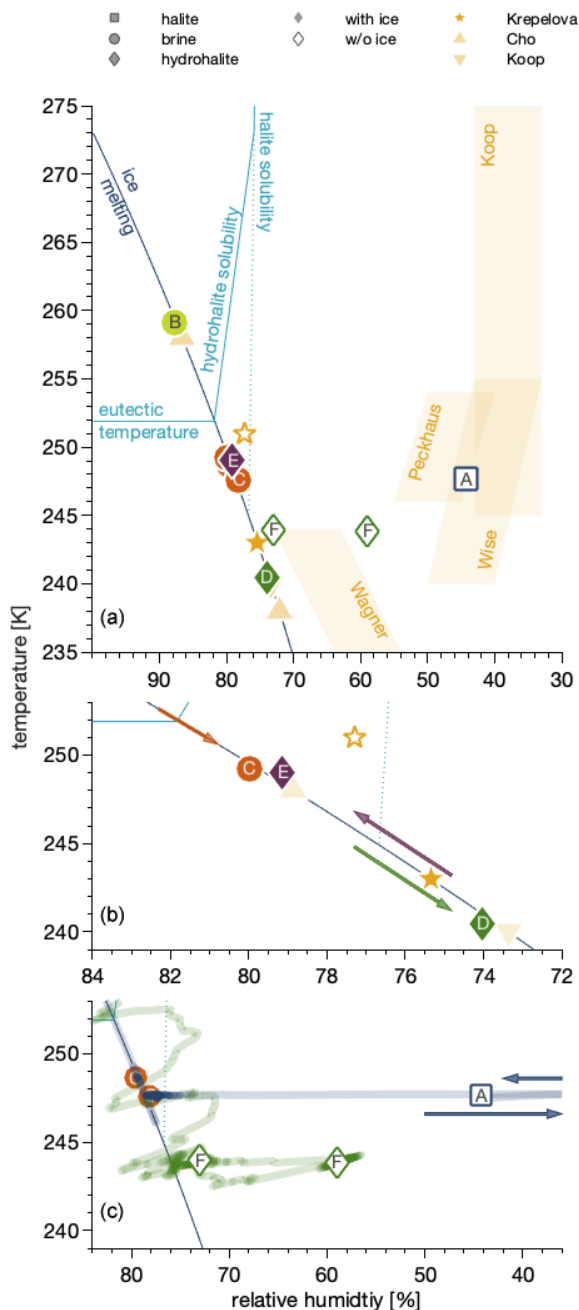


**Figure 4.** Phase diagram of the sodium chloride–water binary system showing the conditions and trajectories of the data in Fig. 3 in the relative humidity–temperature space. The relative humidity is the partial pressure of water relative to the vapour pressure of (supercooled) water as parameterized by Marti and Mauersberger (1993). The dark-blue line denotes settings where ice is stable as the partial pressure of water matches the vapour pressure of ice. Above the eutectic temperature, it thus separates regions where ice and NaCl solution co-exist from those where only NaCl solutions exist. The light-blue lines denote conditions where anhydrous NaCl salt (“halite solubility”) and where NaCl·2H<sub>2</sub>O (“hydrohalite solubility”) form a solution when increasing the relative humidity at constant temperature and where NaCl·2H<sub>2</sub>O dissolves with increasing temperature at a constant relative humidity (“eutectic temperature”). **(a)** Data from this work compared to previous results (Krepelova et al., 2010a; Cho et al., 2002; Koop et al., 2000a). Also shown, as shaded areas, are the data ranges where efflorescence has been observed in earlier work (Koop et al., 2000a; Wagner et al., 2011; Wise et al., 2012; Peckhaus et al., 2016). **(b)** Enlarged view of data below the eutectic temperature. The arrows show the sequence of changes in experimental temperature and relative humidity conditions. **(c)** Enlarged view of the data in the absence of ice. The lines indicate the relative humidity and temperature trajectories to reach the experimental conditions for these data points. The arrows illustrate that the relative humidity was reduced to 0 % prior to returning to the conditions of the measurement.

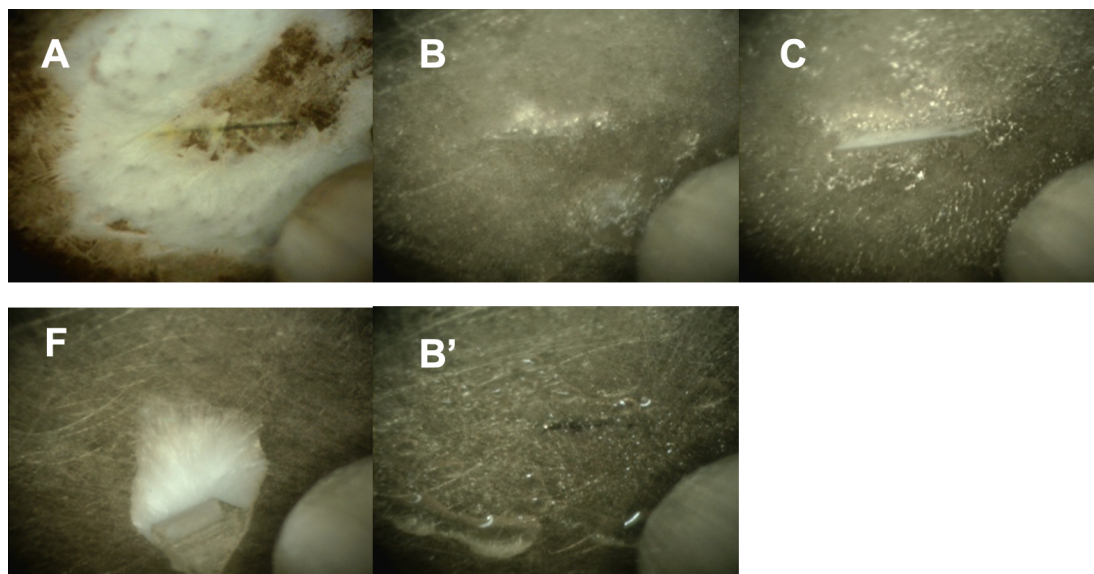


**Figure 5.** Optical microscopy pictures of the frozen samples. Each picture shows a 1 mm wide section of the sample holder with the sample. The letters refer to the samples in Figs. 3 and 4: Sample A – solid NaCl at 248 K and 44 % relative humidity. Sample B – ice with brine at 88 % RH and 259 K. Picture B' shows the deliquesced sample prior to freezing. Sample C – sample below the eutectic temperature at 248 to 249 K in the presence of ice. Sample F – sample in the absence of ice at a relative humidity lower than 73 % and at 244 K. Pictures of samples D and E were not taken.

relative humidity space (Fig. 4) as initially constructed by Koop et al. (2000a). In this work, the relative humidity (RH) is referenced to the vapour pressure of (supercooled) water as parameterized by Marti and Mauersberger (1993). There are two sets of experiments, those where ice is present – and the sodium chloride is in equilibrium with ice (filled symbols) – and experiments in the absence of ice (open symbols) that were performed with a relative humidity of less than the ice stability line in the phase diagram (dark-blue line).

### 3.3 Liquid below eutectic temperature and nucleation

In a typical experiment, anhydrous salt was exposed to increased relative humidity at a fixed temperature of 259 K. Once the relative humidity reached 72 %, the sample started to dissolve by water uptake from the gas phase and an aqueous solution was formed (brine). This phase change was evident by the sample becoming shiny and then forming transparent spheres as observed by an endoscope digital camera (Fig. 5, picture B'). Then, the relative humidity was further increased to cross the ice stability line until ice nucleation occurred at a modest supersaturation of typically 90 % to 95 % relative humidity at 259 K. This relative humidity range corresponds to a supersaturation with respect to ice of 103 % to 109 %. Ice nucleation was evident by a sharp pressure drop from the pressure dosed to the cell to the water vapour pressure of ice at that temperature, for example 88 % relative humidity at 259 K. In some experiments, temperature was lowered by 1 to 2 K as well to trigger ice nucleation. Please note that temperature was always well above the homoge-

nous freezing temperature, which was found at 210 to 230 K at a relative humidity of 60 % to 90 % (Koop et al., 2000a). Generally, in the presence of ice, the partial pressure of water in the flow-through cell is given by the vapour pressure of ice and is thus a sole function of temperature. If the water vapour pressure upstream of the flow-through cell exceeds this value, the ice on the sample holder is growing; if it is set below this value, the ice sublimates. Based on the calibration of the dosing reservoir temperature and partial pressure of water in the flow-through cell (in the absence of ice), the incoming H<sub>2</sub>O vapour flux was adjusted such that the equilibrium pressure in the cell matched the vapour pressure of ice.

A NEXAFS spectrum was acquired at 259 K and 1.82 mbar on the ice stability line and taken as the reference for aqueous sodium chloride solutions (Fig. 3b). When the temperature was lowered while adapting the flux of water into the set-up to match the vapour pressure of ice at 248–249 K, thus 3 to 4 K below the eutectic temperature (Fig. 4b), the NEXAFS spectra revealed that the chloride at the air-ice interface is in an environment identical to that of aqueous chloride (Fig. 3c). While cooling further and adjusting the vapour pressure to match that of ice at each temperature, a sudden change in the sample appearance, becoming less transparent, was observed by the digital endoscope, indicating efflorescence of the sample. A recorded NEXAFS spectrum reveals that hydrohalite has precipitated from the brine at 241 K and 74 % RH (Fig. 3d). Krepelova et al. (2010a) have studied phase changes of sodium chloride at the in-

terfacial region of sodium chloride–water binary mixtures previously. They have probed the oxygen with XPS and by partial electron yield NEXAFS spectroscopy and concluded that, in the presence of ice, hydrohalite forms at about 11 K below the eutectic temperature (filled star in Fig. 4). Consistent with that, the chloride has a local environment indistinguishable from that of the hydrohalite 11.4 K below the eutectic temperature and in the presence of ice in the current study (Fig. 3d). Our results of precipitation in the presence of ice surfaces agree with the crystallization temperature observed by Koop et al. (2000a). We lack a direct comparison to the bulk, because the electron yield NEXAFS spectroscopy used in our work is inherently surface sensitive. Cooling sodium chloride solutions of varying concentration, Koop et al. (2000a) found precipitation of hydrohalite at 240 K in the presence of ice for bulk samples. Because precipitation occurred at 20 K higher temperatures compared to emulsion samples of the same concentration, the authors concluded that the presence of surfaces enhances the crystallization rate. In that study, the hydrohalite was identified by the melting temperatures of the ice–hydrohalite mixtures. Malley et al. (2018) observed crystallization of sodium chloride solutions at 1 K below the eutectic temperature in the presence of ice. The hydrohalite was clearly identified using bulk-sensitive Raman spectroscopy. This difference in crystallization temperature may reflect the stochastic character of freezing, as already noted by Koop et al. (2000a) when discussing the scatter in their data. The precise crystallization temperature is also influenced by the freezing rate, concentration, and the availability of surfaces (Bartels-Rausch et al., 2014). It thus appears that the precise occurrence of crystallization is governed by stochastics at the surface as has been shown for freezing of bulk samples (Alpert and Knopf, 2016) and by experimental settings. Because of the good agreement between the precipitation temperatures observed in this study and in Koop et al. (2000a), we believe that the deviation from the results of Malley et al. (2018) does not indicate differences in the freezing behaviour at the surface vs. that in the bulk.

To investigate the impact of the sample's history on the phase, the sample at 241 K (filled green diamond, Fig. 4b) was warmed towards the eutectic temperature while staying in the ice stability domain. Acquiring a NEXAFS spectrum 3 K below the eutectic temperature (Fig. 3e) that resembles that of hydrohalite shows that liquid brine is not the thermodynamically stable form at temperatures close to the eutectic. We therefore interpret the existence of liquid during the previous cooling of the sample (Fig. 4b, orange circle; Fig. 3c) at the interface as supercooled solution. The sample was kept at this condition for 3 h. This shows that liquid can exist for extended times at the air–ice interface below the eutectic temperature and that the temperature alone is not sufficient to predict its presence. Rather the thermal history of the frozen matrix needs to be considered.

For samples that were cooled to temperatures that triggered efflorescence, the chlorine NEXAFS spectra show that the hydrohalite is the dominating phase at the interface of frozen sodium chloride–water binary mixtures. Cho et al. (2002) have shown that when frozen aqueous solutions were warmed, a liquid fraction was observed below the eutectic temperatures. In their experiments, ice was frozen in NMR tubes lowering the temperature to 228 K in 15 min, which is significantly colder than the efflorescence temperatures observed here and by Koop et al. (2000a). After 10 min, the samples were warmed and NMR signals were recorded. Interestingly, Cho et al. (2002) have observed the liquid fraction only in experiments where the sodium chloride concentration in the initial aqueous solution was below  $0.01 \text{ mol L}^{-1}$ . If the initial aqueous solution had a concentration of  $0.5 \text{ mol L}^{-1}$ , no indication of liquid features below the eutectic temperature were found. Tasaki et al. (2010) have shown a similar concentration dependence for sodium bromide solutions using X-ray absorption, reporting solvated bromide in the bulk of the samples below the eutectic temperature only for concentrations below  $50 \text{ mmol L}^{-1}$ .

We will now detail the concentration of brine in the study presented here to elaborate if differences in concentration might explain the differences in the observed liquid content of sub-eutectic samples. The experiments described here started the freezing process with an aqueous solution that was formed in situ and was kept in equilibrium with a vapour pressure of roughly 1.9 mbar. The chloride concentration in such solutions is close to the concentration in a solution at 1.8 mbar and at 259 K, where ice nucleation occurred and where the freezing-point depression data give a concentration of  $3.5 \text{ mol L}^{-1}$ . This concentration can be directly compared to the concentration in the initial solutions of Cho et al. (2002), which ranged from below 0.01 to  $0.5 \text{ mol L}^{-1}$ . This back-of-the-envelope calculation thus suggests that the concentration of the solutions from which ice nucleated in the experiments reported here exceeded those described by Cho et al. (2002) for which no liquid fraction was observed.

Next, we discuss how higher concentrations of initial solution might impact the location of brine in the frozen matrix. The concentration of the initial solution from which ice precipitated determines the ice-to-brine ratio after ice formation. This is because the volume of the brine relative to that of ice is given by the water-to-sodium chloride ratio in the initial solution. The concentration of the brine in the presence of ice is a sole function of temperature and not of the initial concentration of the solution. One might speculate that with large amounts of brine relative to ice, that is concentrations of initial solutions from which ice nucleates  $> 0.5 \text{ mol L}^{-1}$ , patches and inclusions are larger in size than for more dilute solutions. The size of these patches or inclusions is of relevance, as surface forces reduce the melting point only for inclusions in the nanometre range (Nye, 1991; Aristov et al., 1997; Christenson, 2001; Bartels-Rausch et al., 2014). The absence of this so-called inverse Köhler effect in larger

patches or inclusions might explain the lack of liquid features both in the results reported here at the interface of ice and in the high-concentration samples of Cho et al. (2002). Support for large patches at the interface when solutions are frozen comes from a number of studies (Krausko et al., 2014; Tokumasu et al., 2016; Lieb-Lappen et al., 2017; Malley et al., 2018). Low-temperature scanning electron microscopy work suggested the ice surface of frozen  $0.05 \text{ mol L}^{-1}$  sodium chloride–water mixtures being covered by micrometre-sized brine features (Blackford, 2007; Blackford et al., 2007). Malley et al. (2018) used Raman microscopy of sodium chloride solutions of between  $0.02$ – $0.6 \text{ mol L}^{-1}$  initial concentration to identify micrometre-sized, partially connected patches of liquid covering 11 % to 85 % of the ice surface at temperatures above the eutectic temperature. Despite the impact of freezing temperature and rate – which differs among the individual studies – on the distribution of impurities (Bartels-Rausch et al., 2014; Hullar and Anastasio, 2016), these results clearly show the tendency of micrometre-sized features to dominate at the air–ice interface. In the dominant presence of nano-inclusions, we would also expect the deliquescence to occur at a lower temperature. This was not observed in our experiments, suggesting the absence of nano-inclusions in the experiments presented here in the interfacial region. Please note that the NEXAFS spectroscopy presented here probes an area at the interface of the sample with a diameter of about  $500 \mu\text{m}$ . As the spectroscopy is selective to chlorine, we have no information about the fraction of ice in the probed part of the sample.

The previous argumentation is based on the features in the NEXAFS spectrum of sodium chloride–ice mixtures shown in Fig. 3d and e being dominated by the hydrohalite as seen in the NEXAFS spectrum shown in Fig. 3f. In particular the spectrum in Fig. 3e, acquired 3 K below the eutectic temperature, shows a shoulder starting at 2823 eV. Such a feature is absent in the spectrum of the hydrohalite (Fig. 3f), but the spectrum of brine (Fig. 3b) shows an increase in absorption starting at this X-ray energy level. This feature might thus indicate small amounts of brine, and we can thus not exclude the presence of brine in the samples where the hydrohalite dominates the NEXAFS. Given the spectra quality and the small difference in the shape of the liquid and of the hydrohalite spectrum, it is beyond the scope of this work to elaborate whether the NEXAFS spectrum in Fig. 3e might be understood by deconvoluting it into its hydrohalite and brine components and by this reveal a fraction of the chloride being embedded in a brine-like hydrogen-bonding network. Two reasons might explain the presence of liquid-like features in the NEXAFS spectra at sub-eutectic temperatures. First, one might expect a certain distribution in the size of micropockets and a fraction of the pockets might thus be small enough to stabilize liquid at these temperatures. Secondly, some of the chloride might form solvation shells with water molecules from the ice matrix as proposed for trace gases adsorbed to ice (Krepelova et al., 2010b, 2013; Bartels-

Rausch et al., 2017). In particular, we have recently reported chloride-forming solvation shells in the interfacial region of ice upon adsorption of HCl at 253 K (Kong et al., 2017). The surface concentration as derived from XPS suggested that this previous work was done in the stability domain of ice; i.e. the concentration of HCl was too low to melt the ice. Oxygen K-edge NEXAFS spectra showed that a substantial fraction of the water molecules at the air–ice interface is arranged in a hydrogen-bonding structure like that of liquid water. We would like to note that the oxygen K-edge spectra of sodium chloride–ice of Krepelova et al. (2010a) did not reveal water molecules being coordinated like they are (generally speaking) in the liquid. Taken together, the signal from the hydrohalite by far exceeds the signal from chloride in brine or in a liquid-like environment at the molecular level.

### 3.4 Nucleation in the absence of ice

Hydrohalite can also precipitate in the absence of ice by evaporating water from a solution at temperatures below 273 K (Craig et al., 1975; Yang et al., 2017). Such a trajectory, that is the temperature and water vapour pressure the sample experienced, is shown in Fig. 4c (solid green line). In this set of experiments, water was evaporated by decreasing the relative humidity to about 70 % at 252 K from a brine sample in the absence of ice, followed by lowering the temperature to 247 K at constant partial pressure of water (so that the relative humidity increased to about 80 %). When the ice stability line in the phase diagram was crossed, ice nucleation was not observed as the oversaturation was not sufficient to trigger ice nucleation. This procedure was repeated to further lower the temperature to 244 K at 59 % relative humidity. Then, the first NEXAFS was recorded at 244 K and 59 % RH (Fig. 4, green diamond), where in the absence of ice, nucleation was visually observed. The location in the phase diagram is in agreement with the observation of Wagner et al. (2012) of salt deposits in aerosol droplets in an aerosol chamber (AIDA) in the absence of ice. The second NEXAFS spectrum was recorded at a slightly higher relative humidity of 73 % (Fig. 4, green diamond). Both NEXAFS spectra (Fig. 4, green diamonds) were identified as hydrohalite (Fig. 3f).

The sample at 44 % RH (Fig. 3a) was exposed to 0 % RH prior to acquiring the NEXAFS spectrum (Fig. 4c, blue square and blue line), which removes the crystal water (Light et al., 2009; Wise et al., 2012). This NEXAFS spectrum recorded at 248 K and 44 % RH shows that no deliquescence occurred and thus serves as a reference for a halite spectrum (Fig. 3a). We note that we misinterpreted this spectrum as that of hydrohalite in our previous technical paper introducing the NAPP end station (Orlando et al., 2016). The halite spectrum (Fig. 3a; Fig. 4c, blue square) was recorded at 44 % RH, a humidity where water readily adsorbs on surfaces (Bluhm, 2010), and the presence of water at the sodium chloride–air interface at elevated RH has been demonstrated

previously (Ewing, 2005; Wise et al., 2008). A further reason for the presence of water at lower RH than that of the deliquescence might be sodium chloride's high solubility. Kong et al. (2020) have recently suggested that sodium ions from sodium acetate are dissolved in adsorbed water prior to deliquescence. Indications for solvation of halide ions on single crystals below deliquescence relative humidity have also been reported previously (Luna et al., 1998). An analogue investigation was beyond the scope of this work. The fact that we find no indication for a dominant liquid feature in the upper 6 nm of the sodium chloride–air interface based on the chlorine X-ray absorption spectrum might be due to probing deeper into the interfacial region in this work as compared to that of Kong et al. (2020).

### 3.5 NaCl or NaCl·2H<sub>2</sub>O

We have shown that in the presence of ice, hydrohalite precipitates; halite was not observed in this study except when crystal water was removed in vacuum. This agrees with Koop et al. (2000a), who found precipitation of hydrohalite in the presence of ice and suggested that heterogenous nucleation at ice surfaces favours nucleation of hydrohalite. Studies with liquid droplets in the absence of ice found both halite and hydrohalite precipitating in the thermodynamic stability domain of the hydrohalite (Wagner et al., 2011; Wise et al., 2012; Peckhaus et al., 2016). The transition between crystallization of halite and hydrohalite at between 253 and 241 K was explained based on nucleation theory and the deviating trend of the nucleation rate of both species with temperature (Peckhaus et al., 2016). That hydrohalite crystallizes in the absence of ice in our study shows that gold surfaces, of the sample holder, also serve as good nucleation support for hydrohalite. It appears that any specific properties of the ice surface, as compared to gold, are of minor importance. In agreement, Wagner et al. (2015) showed efficient nucleation of hydrohalite in droplets containing solid oxalic acid and halite precipitated in the absence of oxalic acid at the same temperature and relative humidity.

## 4 Summary and atmospheric implication

The upper few nanometres (mean electron escape depth of 6 nm) of the interfacial region of a sodium chloride–ice binary system was investigated in this study at various positions in the phase diagram. The sample was always in equilibrium with gas-phase water which makes cooling conditions identical and the concentration of brine similar to that of aerosol particles embedded in snow or in the troposphere. The inherent sensitivity to the interfacial region comes from using partial Auger–Meitner electron yield NEXAFS spectroscopy and the limited pathlength of electrons travelling in matter. With a mean electron escape depth of 6 nm, the interfacial region is probed spanning the upper molecular layers

to somewhat into the bulk (Ammann et al., 2018). In this work, we describe the NEXAFS spectrum of hydrohalite for the first time.

The results emphasize that the nucleation of hydrohalite is a function of both the temperature and the relative humidity. While we show that the nucleation of hydrohalite at the interface is favoured by surfaces, we find supercooled solutions of sodium chloride in the interfacial region of ice. The supercooled solutions have been observed to be metastable for hours in these experiments. This has direct implications for heterogeneous chemistry in cold parts of Earth's environment. Multiphase reactions may proceed at accelerated rates in these highly concentrated brines at temperatures  $\sim 10^\circ\text{C}$  below the eutectic temperature compared to reactions on solid hydrohalite. This temperature range of  $\sim 241\text{ K}$  is frequently observed in polar coastal sites during spring and in the free troposphere. In this respect, there is no difference in the interfacial region to liquid embedded in the bulk of snow and ice samples. This implies that when chemical reactivity of ice and snow is discussed, knowledge of its thermal history is essential. From temperature and relative humidity alone, nucleation or efflorescence cannot be predicted at the interface just like in the bulk. We suggest that further studies focus on samples with more complex chemical composition to enhance our knowledge of environmental multiphase chemistry. For example, organic compounds are a common constituent of sea-salt aerosols (O'Dowd et al., 2004). Kirpes et al. (2019) and Edebeli et al. (2019) have shown how the presence of organics impacts the microphysics of salt particles and thus their reactivity towards ozone. Further, Chakraborty and Kahan (2020) have shown a depression in hydrohalite precipitation temperature in humic acid–sodium chloride mixtures.

We suggest that the brine observed by Cho et al. (2002) is a consequence of the presence of very small pockets holding the brine. Because pockets only tend to be small enough to establish a significant depression in the freezing point when solutions with low concentration are freezing and because aerosols at typical relative humidity that prevail in cold parts of the atmosphere are highly concentrated, we suggest that such nano-pockets at the air–ice interface are of small relevance to the environment.

The appearance of hydrohalite at air–ice interfaces might also be of interest to sea ice research, because precipitation of hydrohalite increases the albedo of sea ice. During the snowball Earth period, 700 million years before present, climatic conditions may have favoured the existence of hydrohalite with its climatic feedback (Light et al., 2009). For modern Earth, precipitation of brine constituents in sea ice is relevant for ion mobility and might result in ion fractionation during washout events (Maus et al., 2008; Obbard et al., 2009; Maus et al., 2011) and possibly brine migration upwards through the snow (Dominé et al., 2004).

Precipitation of sodium chloride in sea spray aerosols in the troposphere, not embedded in snow or sea ice, is of fur-

ther ongoing interest. Again, the Arctic coastal areas are of high relevance here, because temperature and relative humidity frequently favour precipitation of hydrohalite. Other studies have focused on the temperature range of 230 to 260 K at a relative humidity of 30 % to 70 % (see Fig. 4 and references therein) to explore the precipitation in the dryer free troposphere. Research has focused on whether anhydrous sodium chloride (halite) or hydrohalite precipitates. In regions of the phase diagram, where the hydrohalite is the thermodynamic stable form, precipitation of the halite was observed with impacts on stability of the solid phase upon warming and/or humidification, since the deliquesce relative humidity of the two compounds differs by 6 percentage points (Wagner et al., 2012; Wise et al., 2012; Peckhaus et al., 2016).

## Appendix A

The spectra in Fig. A1 can be described as follows:

- The Na1s region shows one Gaussian shaped feature at 1072 eV as expected for sodium.
- The O1s region shows one dominant feature at 535 eV in line with oxygen in ice and a smaller feature at higher binding energy which might be attributed to gas-phase water.
- The Cl2p region shows the typical doublet of the p-orbital spin-orbit splitting ( $p(3/2)$  and  $p(1/2)$ ), 1.6 eV apart at 200 eV binding energy. Additionally, in some spectra a small feature at 203 eV binding energy is evident which might be attributed to the Cl2p(1/2) of organic carbon species.
- The C1s region shows a broad spectrum with the main feature at 285 eV binding energy, typical of the C–H of adventitious carbon. The overlapping features at higher binding energy can be attributed to C–OH, C=O, C(O)=O, and C–Cl.
- The spectra of all species acquired before and after the sample in Fig. A1 are significantly wider compared to the other samples. Additionally, the Cl2p features are shifted by 2 eV to a lower binding energy. This sample is, unlike the others, characterized by a large variation in sample thickness (Fig. 3a) which leads to differential charging and might explain the wider peak shapes and shift in the Cl2p features.
- In sample A, the photoemission intensities of the Na1s and Cl2p show a higher intensity after the NEXAFS spectrum was acquired compared to before. During that time, the photoemission intensity of O1s increased. This suggests that water kept adsorbing to the sample and masked the signal intensity of the underlying sodium chloride.
- In sample B, all photoemission intensities decreased during the time it took to acquire the NEXAFS spectra. This suggests that the working distances changed which impacts the sensitivity of all sample components.

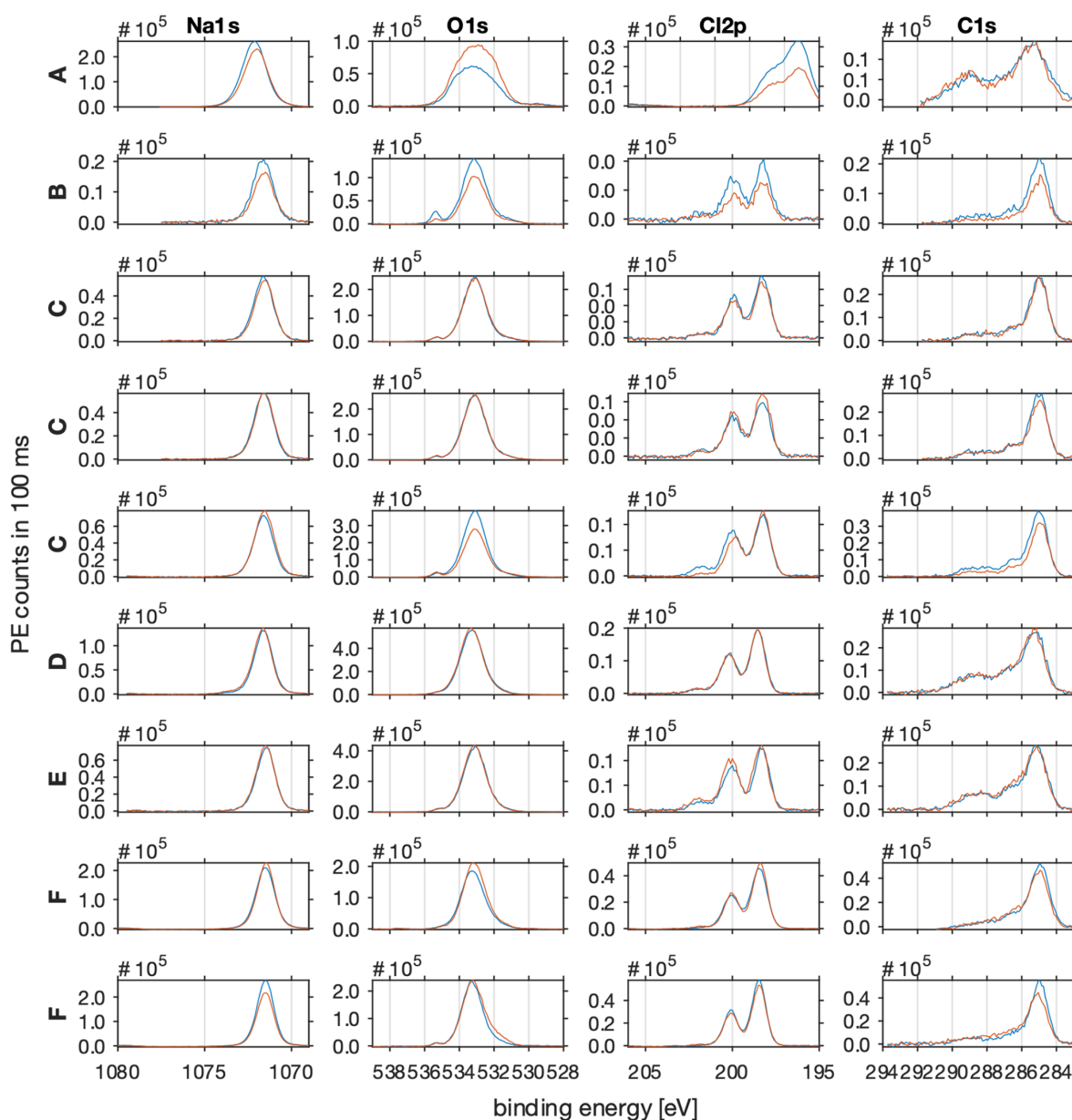


**Figure A1.** The photo emission intensities as acquired before (blue line) and after (red line) each NEXAFS spectrum. The photo emission (PE) spectra of sodium (Na1s) are shown in column 1, of oxygen (O1s) in column 2, of chlorine (Cl2p) in column 3, and of carbon (C1s) in column 4. All spectra were acquired at the PHOENIX beamline of SLS of the PSI with a photon energy of 2200 eV. Pass energy was set to 100 eV and dwell time to 100 ms. Beamline slits were  $2 \times 2$  mm. The C–H feature at 285 eV of the C1s photoemission spectra served as the binding-energy reference, and all spectra were shifted by 4–5.5 eV to account for charging effects.

## Appendix B

**Table B1.** Freezing-point depression data of NaCl (Rumble, 2019).

Mass fraction [%]	Molal concentration [mol kg <sup>-1</sup> ]	Molar concentration [mol L <sup>-1</sup> ]	Freezing depression [K]
0.1	0.017	0.017	0.06
0.2	0.034	0.034	0.12
0.3	0.051	0.051	0.18
0.4	0.069	0.069	0.24
0.5	0.086	0.086	0.3
1	0.173	0.172	0.59
1.5	0.261	0.259	0.89
2	0.349	0.346	1.19
2.5	0.439	0.435	1.49
3	0.529	0.523	1.79
3.5	0.621	0.613	2.1
4	0.713	0.703	2.41
4.5	0.806	0.793	2.73
5	0.901	0.885	3.05
6	1.092	1.069	3.7
7	1.288	1.256	4.38
8	1.488	1.445	5.08
9	1.692	1.637	5.81
10	1.901	1.832	6.56
11	2.115	2.029	7.35
12	2.333	2.229	8.18
13	2.557	2.432	9.04
14	2.785	2.637	9.94
15	3.02	2.845	10.89
16	3.259	3.056	11.89
17	3.505	3.27	12.94
18	3.756	3.486	14.04
19	4.014	3.706	15.22
20	4.278	3.928	16.46
21	4.548	4.153	17.78
22	4.826	4.382	19.18
23	5.111	4.613	20.67

**Data availability.** Data are available at the EnviDat repository: <https://doi.org/10.16904/envidat.164> (Bartels-Rausch, 2020) – a data set on interfacial supercooling and the precipitation of hydrohalite in frozen NaCl solutions by X-ray absorption spectroscopy.

**Author contributions.** TBR designed and planned the study, analysed the data, and wrote the manuscript. FO, LA, MA, and TH planned and optimized beamline and electron analyser settings. XK, AW, LA, and TBR performed the experiments. All authors approved the submitted version of the manuscript.

**Competing interests.** The authors declare that they have no conflict of interest.

**Acknowledgements.** Funding by the Swiss National Science Foundation (SNSF) under grant no. 149629 is acknowledged. We thank Mario Birrer (PSI) for his technical assistance. Thorsten Bartels-Rausch thanks Peter Alpert for stimulating discussion in the office. We thank the SLS team and PHOENIX beamline team for their assistance and for providing a stable and brilliant beam.

**Financial support.** This research has been supported by the Schweizerischer Nationalfonds zur Förderung der wissenschaftlichen Forschung (grant no. 149629).

**Review statement.** This paper was edited by Florent Dominé and reviewed by Subha Chakraborty and two anonymous referees.

## References

- Abbatt, J. P. D., Thomas, J. L., Abrahamsson, K., Boxe, C., Granfors, A., Jones, A. E., King, M. D., Saiz-Lopez, A., Shepson, P. B., Sodeau, J., Toohey, D. W., Toubin, C., von Glasow, R., Wren, S. N., and Yang, X.: Halogen activation via interactions with environmental ice and snow in the polar lower troposphere and other regions, *Atmos. Chem. Phys.*, 12, 6237–6271, <https://doi.org/10.5194/acp-12-6237-2012>, 2012.
- Alpert, P. A. and Knopf, D. A.: Analysis of isothermal and cooling-rate-dependent immersion freezing by a unifying stochastic ice nucleation model, *Atmos. Chem. Phys.*, 16, 2083–2107, <https://doi.org/10.5194/acp-16-2083-2016>, 2016.
- Ammann, M., Artiglia, L., and Bartels-Rausch, T.: X-ray excited electron spectroscopy to study gas–liquid interfaces of atmospheric relevance, in: *Physical chemistry of gas–liquid interfaces*, Elsevier, 135–166, 2018.
- Antalek, M., Pace, E., Hedman, B., Hodgson, K. O., Chillemi, G., Benfatto, M., Sarangi, R., and Frank, P.: Solvation structure of the halides from x-ray absorption spectroscopy, *J. Chem. Phys.*, 145, 044318, <https://doi.org/10.1063/1.4959589>, 2016.
- Aristov, Y. I., Di Marco, G., Tokarev, M. M., and Parmon, V. N.: Selective water sorbents for multiple applications, 3. CaCl<sub>2</sub> solution confined in micro- and mesoporous silica gels: Pore size effect on the “solidification-melting” diagram, *React. Kinet. Catal. Lett.*, 61, 147–154, <https://doi.org/10.1007/BF02477527>, 1997.
- Artiglia, L., Edebeli, J., Orlando, F., Chen, S., Lee, M.-T., Corral Arroyo, P., Gilgen, A., Bartels-Rausch, T., Kleibert, A., Vazdar, M., Carignano, M. A., Francisco, J. S., Shepson, P. B., Gladich, I., and Ammann, M.: A surface-stabilized ozonide triggers bromide oxidation at the aqueous solution-vapour interface, *Nat. Commun.*, 8, 700, <https://doi.org/10.1038/s41467-017-00823-x>, 2017.
- Bartels-Rausch, T.: Data set on interfacial supercooling and the precipitation of hydrohalite in frozen NaCl solutions by X-ray absorption spectroscopy, *EnviDat*, <https://doi.org/10.16904/envidat.164>, 2020.
- Bartels-Rausch, T., Jacobi, H.-W., Kahan, T. F., Thomas, J. L., Thomson, E. S., Abbott, J. P. D., Ammann, M., Blackford, J. R., Bluhm, H., Boxe, C., Domine, F., Frey, M. M., Gladich, I., Guzmán, M. I., Heger, D., Huthwelker, Th., Klán, P., Kuhs, W. F., Kuo, M. H., Maus, S., Moussa, S. G., McNeill, V. F., Newberg, J. T., Pettersson, J. B. C., Roeselová, M., and Sodeau, J. R.: A review of air–ice chemical and physical interactions (AICI): liquids, quasi-liquids, and solids in snow, *Atmos. Chem. Phys.*, 14, 1587–1633, <https://doi.org/10.5194/acp-14-1587-2014>, 2014.
- Bartels-Rausch, T., Orlando, F., Kong, X., Artiglia, L., and Ammann, M.: Experimental evidence for the formation of solvation shells by soluble species at a nonuniform air-ice interface, *ACS Earth Space Chem.*, 1, 572–579, <https://doi.org/10.1021/acsearthspacechem.7b00077>, 2017.
- Blackford, J. R.: Sintering and microstructure of ice: A review, *J. Phys. D*, 40, R355–R385, <https://doi.org/10.1088/0022-3727/40/21/R02>, 2007.
- Blackford, J. R., Jeffree, C. E., Noake, D. F. J., and Marmo, B. A.: Microstructural evolution in sintered ice particles containing NaCl observed by low-temperature scanning electron microscope, *Proc. Inst. Mech. Eng.*, 221, 151–156, <https://doi.org/10.1243/14644207JMDA134>, 2007.
- Bluhm, H., Ogletree, D. F., Fadley, C. S., Hussain, Z., and Salmeron, N.: The premelting of ice studied with photoelectron spectroscopy, *J. Phys.: Condens. Matter*, 14, L227–L233, <https://doi.org/10.1088/0953-8984/14/8/108>, 2002.
- Bluhm, H.: Photoelectron spectroscopy of surfaces under humid conditions, *J. Electron Spectrosc.*, 177, 71–84, <https://doi.org/10.1016/j.elspec.2009.08.006>, 2010.
- Chakraborty, S. and Kahan, T. F.: Physical characterization of frozen aqueous solutions containing sodium chloride and humic acid at environmentally relevant temperatures, *ACS Earth Space Chem.*, 4, 305–310, <https://doi.org/10.1021/acsearthspacechem.9b00319>, 2020.
- Cho, H., Shepson, P. B., Barrie, L. A., Cowin, J. P., and Zaveri, R.: NMR investigation of the quasi-brine layer in ice/brine mixtures, *J. Phys. Chem. B*, 106, 11226–11232, <https://doi.org/10.1021/jp020449+>, 2002.
- Christenson, H. K.: Confinement effects on freezing and melting, *J. Phys.*, 13, R95–R133, <https://doi.org/10.1088/0953-8984/13/11/201>, 2001.
- Cleff, B. and Mehlhorn, W.: Das KLL- Auger-Spektrum von Chlor, *Z. Phys. A*, 219, 311–324, <https://doi.org/10.1007/BF01395528>, 1969.
- Craig, J. R., Light, J. F., Parker, B. C., and Mudrey, M. G.: Identification of hydrohalite, *Antarct. J. US*, 10, 178–179, 1975.

- Custard, K. D., Raso, A. R. W., Shepson, P. B., Staebler, R. M., and Pratt, K. A.: Production and release of molecular bromine and chlorine from the arctic coastal snowpack, *ACS Earth Space Chem.*, 1, 142–151, <https://doi.org/10.1021/acsearthspacechem.7b00014>, 2017.
- Dominé, F. and Shepson, P. B.: Air-snow interactions and atmospheric chemistry, *Science*, 297, 1506–1510, <https://doi.org/10.1126/science.1074610>, 2002.
- Dominé, F., Sparapani, R., Ianniello, A., and Beine, H. J.: The origin of sea salt in snow on Arctic sea ice and in coastal regions, *Atmos. Chem. Phys.*, 4, 2259–2271, <https://doi.org/10.5194/acp-4-2259-2004>, 2004.
- Edebeli, J., Ammann, M., and Bartels-Rausch, T.: Microphysics of the aqueous bulk counters the water activity driven rate acceleration of bromide oxidation by ozone from 289–245 K, *Environ. Sci. Process. Impacts*, 21, 63–73, <https://doi.org/10.1039/c8em00417j>, 2019.
- Evans, K. A., Mavrogenes, J. A., O'Neill, H. S., Keller, N. S., and Jang, L. Y.: A preliminary investigation of chlorine XANES in silicate glasses, *Geochem. Geophys. Geos.*, 9, Q10003, <https://doi.org/10.1029/2008gc002157>, 2008.
- Ewing, G. E.: H<sub>2</sub>O on NaCl: From single molecule, to clusters, to monolayer, to thin film, to deliquescence, chap. 12, Springer-Verlag, Berlin/Heidelberg, 1–25, 2005.
- Finlayson-Pitts, B. J.: The tropospheric chemistry of sea salt: A molecular-level view of the chemistry of NaCl and NaBr, *Chem. Rev.*, 103, 4801–4822, <https://doi.org/10.1021/cr020653t>, 2003.
- Finlayson-Pitts, B. J.: Halogens in the troposphere, *Anal. Chem.*, 82, 770–776, <https://doi.org/10.1021/ac901478p>, 2010.
- Fujimori, T., Takaoka, M., and Morisawa, S.: Chlorinated aromatic compounds in a thermal process promoted by oxychlorination of ferric chloride, *Environ. Sci. Technol.*, 44, 1974–1979, <https://doi.org/10.1021/es903337d>, 2010.
- Gladich, I., Chen, S., Vazdar, M., Boucly, A., Yang, H., Ammann, M., and Artiglia, L.: Surface propensity of aqueous atmospheric bromine at the liquid-gas interface, *J. Phys. Chem. Lett.*, 11, 3422–3429, <https://doi.org/10.1021/acs.jpcclett.0c00633>, 2020.
- Grannas, A. M., Bausch, A. R., and Mahanna, K. M.: Enhanced aqueous photochemical reaction rates after freezing, *J. Phys. Chem. A*, 111, 11043–11049, <https://doi.org/10.1021/jp073802q>, 2007.
- Halfacre, J. W., Shepson, P. B., and Pratt, K. A.: pH-dependent production of molecular chlorine, bromine, and iodine from frozen saline surfaces, *Atmos. Chem. Phys.*, 19, 4917–4931, <https://doi.org/10.5194/acp-19-4917-2019>, 2019.
- Harada, M., Tasaki, Y., Tasaki, Y., Qu, H., and Okada, T.: Hydration of ions and salt crystallization in liquid phase coexistent with ice at temperature below eutectic point, *RSC Advances*, 2, 461–466, <https://doi.org/10.1039/c1ra00801c>, 2011.
- Huggins, F. E. and Huffman, G. P.: Chlorine in coal – an XAFS spectroscopic investigation, *Fuel*, 74, 556–569, [https://doi.org/10.1016/0016-2361\(95\)98359-m](https://doi.org/10.1016/0016-2361(95)98359-m), 1995.
- Hullar, T. and Anastasio, C.: Direct visualization of solute locations in laboratory ice samples, *The Cryosphere*, 10, 2057–2068, <https://doi.org/10.5194/tc-10-2057-2016>, 2016.
- Kahan, T. F., Wren, S. N., and Donaldson, D. J.: A pinch of salt is all it takes: Chemistry at the frozen water surface, *Acc. Chem. Res.*, 47, 1587–1594, <https://doi.org/10.1021/ar5000715>, 2014.
- Kirpes, R. M., Bonanno, D., May, N. W., Fraund, M., Barget, A. J., Moffet, R. C., Ault, A. P., and Pratt, K. A.: Wintertime arctic sea spray aerosol composition controlled by sea ice lead microbiology, *ACS Cent. Sci.*, 5, 1760–1767, <https://doi.org/10.1021/acscentsci.9b00541>, 2019.
- Klewe, B., Pedersen, B., and Iucr: The crystal structure of sodium chloride dihydrate, *Acta Crystallogr.*, 30, 2363–2371, <https://doi.org/10.1107/S0567740874007138>, 1974.
- Knipping, E. M., Lakin, M. J., Foster, K. L., Jungwirth, P., Tobias, D. J., Gerber, R. B., Dabdub, D., and Finlayson-Pitts, B. J.: Experiments and simulations of ion-enhanced interfacial chemistry on aqueous NaCl aerosols, *Science*, 288, 301–306, <https://doi.org/10.1126/science.288.5464.301>, 2000.
- Kong, X., Waldner, A., Orlando, F., Artiglia, L., Huthwelker, T., Ammann, M., and Bartels-Rausch, T.: Coexistence of physisorbed and solvated HCl at warm ice surfaces, *J. Phys. Chem. Lett.*, 8, 4757–4762, <https://doi.org/10.1021/acs.jpcclett.7b01573>, 2017.
- Kong, X., Castarède, D., Boucly, A., Artiglia, L., Ammann, M., Bartels-Rausch, T., Thomson, E. S., and Pettersson, J. B. C.: Reversibly physisorbed and chemisorbed water on carboxylic salt surfaces under atmospheric conditions, *J. Phys. Chem. C*, 124, 5263–5269, <https://doi.org/10.1021/acs.jpcc.0c00319>, 2020.
- Koop, T., Kapilashrami, A., Molina, L. T., and Molina, M. J.: Phase transitions of sea-salt/water mixtures at low temperatures: Implications for ozone chemistry in the polar marine boundary layer, *J. Geophys. Res.*, 105, 26393–26402, <https://doi.org/10.1029/2000JD900413>, 2000a.
- Koop, T., Luo, B. P., Tsias, A., and Peter, T.: Water activity as the determinant for homogeneous ice nucleation in aqueous solutions, *Nature*, 406, 611–614, <https://doi.org/10.1038/35020537>, 2000b.
- Krausko, J., Runštuk, J., Neděla, V., Klan, P., and Heger, D.: Observation of a brine layer on an ice surface with an environmental scanning electron microscope at higher pressures and temperatures, *Langmuir*, 30, 5441–5447, <https://doi.org/10.1021/la500334e>, 2014.
- Krepelova, A., Huthwelker, T., Bluhm, H., and Ammann, M.: Surface chemical properties of eutectic and frozen NaCl solutions probed by XPS and NEXAFS, *Chem. Phys. Chem.*, 11, 3859–3866, <https://doi.org/10.1002/cphc.201000461>, 2010a.
- Krepelova, A., Newberg, J. T., Huthwelker, T., Bluhm, H., and Ammann, M.: The nature of nitrate at the ice surface studied by XPS and NEXAFS, *Phys. Chem. Chem. Phys.*, 12, 8870–8880, <https://doi.org/10.1039/c0cp00359j>, 2010b.
- Krepelova, A., Bartels-Rausch, T., Brown, M. A., Bluhm, H., and Ammann, M.: Adsorption of acetic acid on ice studied by ambient-pressure XPS and partial-electron-yield NEXAFS spectroscopy at 230–240 K, *J. Phys. Chem. A*, 117, 401–409, <https://doi.org/10.1021/jp3102332>, 2013.
- Laskin, A., Wang, H., Robertson, W. H., Cowin, J. P., Ezell, M. J., and Finlayson-Pitts, B. J.: A new approach to determining gas-particle reaction probabilities and application to the heterogeneous reaction of deliquesced sodium chloride particles with gas-phase hydroxyl radicals, *J. Phys. Chem. A*, 110, 10619–10627, <https://doi.org/10.1021/jp063263+>, 2006.
- Lieb-Lappen, R. M., Golden, E. J., and Obbard, R. W.: Metrics for interpreting the microstructure of sea ice using X-ray micro-

- computed tomography, *Cold Reg. Sci. Technol.*, 138, 24–35, <https://doi.org/10.1016/j.coldregions.2017.03.001>, 2017.
- Light, B., Brandt, R. E., and Warren, S. G.: Hydrohalite in cold sea ice: Laboratory observations of single crystals, surface accumulations, and migration rates under a temperature gradient, with application to “snowball earth”, *J. Geophys. Res.*, 114, C07018, <https://doi.org/10.1029/2008JC005211>, 2009.
- Lopez-Hilfiker, F. D., Constantin, K., Kercher, J. P., and Thornton, J. A.: Temperature dependent halogen activation by N<sub>2</sub>O<sub>5</sub> reactions on halide-doped ice surfaces, *Atmos. Chem. Phys.*, 12, 5237–5247, <https://doi.org/10.5194/acp-12-5237-2012>, 2012.
- Luna, M., Rieutord, F., Melman, N. A., Dai, Q., and Salmeron, M.: Adsorption of water on alkali halide surfaces studied by scanning polarization force microscopy, *J. Phys. Chem. A*, 102, 6793–6800, <https://doi.org/10.1021/jp9820875>, 1998.
- Malley, P. P. A., Chakraborty, S., and Kahan, T. F.: Physical characterization of frozen saltwater solutions using Raman microscopy, *ACS Earth Space Chem.*, 2, 702–710, <https://doi.org/10.1021/acsearthspacechem.8b00045>, 2018.
- Marti, J. and Mauersberger, K.: A survey and new measurements of ice vapor pressure at temperatures between 170 and 250 K, *Geophys. Res. Lett.*, 20, 363–366, <https://doi.org/10.1029/93GL00105>, 1993.
- Maus, S., Huthwelker, T., Enzmann, F., Miedaner, M. M., Stapanoni, M., Marone, F., Hutterli, M. A., Hintermüller, C., Hintermüller, C., and Kersten, M.: Synchrotron-based X-ray microtomography: Insights into sea ice microstructure, Sixth Workshop on Baltic Sea Ice Climate, Lammi Biological Station, Finland, 2008.
- Maus, S., Huthwelker, T., Schwikowski, M., and Enzmann, F.: Ion fractionation in young sea ice from Kongsfjorden, svalbard, *Ann. Glaciol.*, 52, 301–310, <https://doi.org/10.3189/172756411795931804>, 2011.
- Murphy, D. M., Froyd, K. D., Bian, H., Brock, C. A., Dibb, J. E., DiGangi, J. P., Diskin, G., Dollner, M., Kupc, A., Scheuer, E. M., Schill, G. P., Weinzierl, B., Williamson, C. J., and Yu, P.: The distribution of sea-salt aerosol in the global troposphere, *Atmos. Chem. Phys.*, 19, 4093–4104, <https://doi.org/10.5194/acp-19-4093-2019>, 2019.
- Newberg, J. T. and Bluhm, H.: Adsorption of 2-propanol on ice probed by ambient pressure X-ray photoelectron spectroscopy, *Phys. Chem. Chem. Phys.*, 17, 23554–23558, <https://doi.org/10.1039/C5CP03821A>, 2015.
- Nilsson, A., Nordlund, D., Waluyo, I., Huang, N., Ogasawara, H., Kaya, S., Bergmann, U., Näslund, L. A., Öström, H., Wernet, P., Andersson, K. J., Schiros, T., and Pettersson, L. G. M.: X-ray absorption spectroscopy and X-ray Raman scattering of water and ice; an experimental view, *J. Electron Spectrosc.*, 177, 99–129, <https://doi.org/10.1016/j.elspec.2010.02.005>, 2010.
- Nye, J. F.: Thermal behaviour of glacier and laboratory ice, *J. Glaciol.*, 37, 401–413, <https://doi.org/10.3189/S0022143000005839>, 1991.
- O’Dowd, C. D., Facchini, M. C., Cavalli, F., Ceburnis, D., Mircea, M., Decesari, S., Fuzzi, S., Yoon, Y. J., and Putaud, J.-P.: Biogenically driven organic contribution to marine aerosol, *Nature*, 431, 676–680, <https://doi.org/10.1038/nature02959>, 2004.
- Obbard, R. W., Troderman, G., and Baker, I.: Imaging brine and air inclusions in sea ice using micro-X-ray computed tomography, *J. Glaciol.*, 55, 1113–1115, <https://doi.org/10.3189/002214309790794814>, 2009.
- Oldridge, N. W. and Abbatt, J. P. D.: Formation of gas-phase bromine from interaction of ozone with frozen and liquid NaCl/NaBr solutions: Quantitative separation of surficial chemistry from bulk-phase reaction, *J. Phys. Chem. A*, 115, 2590–2598, <https://doi.org/10.1021/jp200074u>, 2011.
- Orlando, F., Waldner, A., Bartels-Rausch, T., Birrer, M., Kato, S., Lee, M.-T., Proff, C., Huthwelker, T., Kleibert, A., van Bokhoven, J. A., and Ammann, M.: The environmental photochemistry of oxide surfaces and the nature of frozen salt solutions: A new in situ XPS approach, *Top. Catal.*, 59, 591–604, <https://doi.org/10.1007/s11244-015-0515-5>, 2016.
- Osthoff, H. D., Roberts, J. M., Ravishankara, A. R., Williams, E. J., Lerner, B. M., Sommariva, R., Bates, T. S., Coffman, D., Quinn, P. K., Dibb, J. E., Stark, H., Burkholder, J. B., Talukdar, R. K., Meagher, J., Fehsenfeld, F. C., and Brown, S. S.: High levels of nitryl chloride in the polluted subtropical marine boundary layer, *Nat. Geosci.*, 1, 324–328, <https://doi.org/10.1038/ngeo177>, 2008.
- Peckhaus, A., Kiselev, A., Wagner, R., Duft, D., and Leisner, T.: Temperature-dependent formation of NaCl dihydrate in levitated NaCl and sea salt aerosol particles, *J. Chem. Phys.*, 145, 244503, <https://doi.org/10.1063/1.4972589>, 2016.
- Petrich, C. and Eicken, H.: Growth, structure and properties of sea ice, *Sea Ice*, 23–77, <https://doi.org/10.1002/9781444317145.ch2>, 2009.
- Rumble, J.: CRC handbook of chemistry and physics, 100th Edn., CRC Press/Taylor & Francis, Boca Raton, FL., 2019.
- Saiz-Lopez, A. and von Glasow, R.: Reactive halogen chemistry in the troposphere, *Chem. Soc. Rev.*, 41, 6448–6472, <https://doi.org/10.1039/C2CS35208G>, 2012.
- Simpson, W. R., von Glasow, R., Riedel, K., Anderson, P., Ariya, P., Bottenheim, J., Burrows, J., Carpenter, L. J., Frieß, U., Goodsite, M. E., Heard, D., Hutterli, M., Jacobi, H.-W., Kaleschke, L., Neff, B., Plane, J., Platt, U., Richter, A., Roscoe, H., Sander, R., Shepson, P., Sodeau, J., Steffen, A., Wagner, T., and Wolff, E.: Halogens and their role in polar boundary-layer ozone depletion, *Atmos. Chem. Phys.*, 7, 4375–4418, <https://doi.org/10.5194/acp-7-4375-2007>, 2007.
- Simpson, W. R., Brown, S. S., Saiz-Lopez, A., Thornton, J. A., and von Glasow, R.: Tropospheric halogen chemistry: Sources, cycling, and impacts, *Chem. Rev.*, 115, 4035–4062, <https://doi.org/10.1021/cr5006638>, 2015.
- Sjostedt, S. J. and Abbatt, J. P. D.: Release of gas-phase halogens from sodium halide substrates: Heterogeneous oxidation of frozen solutions and desiccated salts by hydroxyl radicals, *Environ. Res. Lett.*, 3, 045007, <https://doi.org/10.1088/1748-9326/3/4/045007>, 2008.
- Tanuma, S., Powell, C. J., and Penn, D. R.: Calculations of electron inelastic mean free paths: 3. Data for 15 inorganic-compounds over the 50–2000 eV range, *Surf. Interface Anal.*, 17, 927–939, <https://doi.org/10.1002/sia.740171305>, 1991.
- Tasaki, Y., Harada, M., and Okada, T.: Eutectic transition of local structure for bromide ion in bulk and on surface of doped ice, *J. Phys. Chem. C*, 114, 12573–12579, <https://doi.org/10.1021/jp102246f>, 2010.
- Thomas, J. L., Stutz, J., Frey, M. M., Bartels-Rausch, T., Altieri, K., Baladima, F., Browse, J., Dall’Osto, M., Marelle, L., Mougnot, J., Jennifer, G. M., Nomura, D., Pratt, K. A., Willis, M. D.,

- Zieger, P., Abbatt, J., Douglas, T. A., Facchini, M. C., France, J., Jones, A. E., Kim, K., Matrai, P. A., McNeill, V. F., Saiz-Lopez, A., Shepson, P., Steiner, N., Law, K. S., Arnold, S. R., Delille, B., Schmale, J., Sonke, J. E., Dommergue, A., Voisin, D., Melamed, M. L., and Gier, J.: Fostering multidisciplinary research on interactions between chemistry, biology, and physics within the coupled cryosphere-atmosphere system, *Elementa*, 7, 58, doi:10.1525/elementa.396, 2019.
- Thornton, J. A., Kercher, J. P., Riedel, T. P., Wagner, N. L., Cozic, J., Holloway, J. S., Dube, W. P., Wolfe, G. M., Quinn, P. K., Middlebrook, A. M., Alexander, B., and Brown, S. S.: A large atomic chlorine source inferred from mid-continental reactive nitrogen chemistry, *Nature*, 464, 271–274, https://doi.org/10.1038/nature08905, 2010.
- Tokumasu, K., Harada, M., and Okada, T.: X-ray fluorescence imaging of frozen aqueous NaCl solutions, *Langmuir*, 32, 527–533, https://doi.org/10.1021/acs.langmuir.5b04411, 2016.
- Wagner, R., Möhler, O., Saathoff, H., Schnaiter, M., and Leisner, T.: New cloud chamber experiments on the heterogeneous ice nucleation ability of oxalic acid in the immersion mode, *Atmos. Chem. Phys.*, 11, 2083–2110, https://doi.org/10.5194/acp-11-2083-2011, 2011.
- Wagner, R., Mohler, O., and Schnaiter, M.: Infrared optical constants of crystalline sodium chloride dihydrate: Application to study the crystallization of aqueous sodium chloride solution droplets at low temperatures, *J. Phys. Chem. A*, 116, 8557–8571, https://doi.org/10.1021/jp306240s, 2012.
- Wagner, R., Höhler, K., Möhler, O., Saathoff, H., and Schnaiter, M.: Crystallization and immersion freezing ability of oxalic and succinic acid in multicomponent aqueous organic aerosol particles, *Geophys. Res. Lett.*, 42, 2464–2472, https://doi.org/10.1002/2015GL063075, 2015.
- Waldner, A., Artiglia, L., Kong, X., Orlando, F., Huthwelker, T., Ammann, M., and Bartels-Rausch, T.: Pre-melting and the adsorption of formic acid at the air–ice interface at 253 K as seen by NEXAFS and XPS, *Phys. Chem. Chem. Phys.*, 20, 24408–24417, https://doi.org/10.1039/C8CP03621G, 2018.
- Wang, S., Schmidt, J. A., Baidar, S., Coburn, S., Dix, B., Koenig, T. K., Apel, E. C., Bowdalo, D., Campos, T. L., Eloranta, E., Evans, M. J., DiGangi, J. P., Zondlo, M. A., Gao, R.-S., Haggerty, J. A., Hall, S. R., Hornbrook, R. S., Jacob, D., Morley, B., Pierce, B., Reeves, M., Romashkin, P., ter Schure, A., and Volkamer, R.: Active and widespread halogen chemistry in the tropical and subtropical free troposphere, *P. Natl. Acad. Sci. USA*, 112, 201505142–201509286, https://doi.org/10.1073/pnas.1505142112, 2015.
- Wise, M. E., Martin, S. T., Russell, L. M., and Buseck, P. R.: Water uptake by NaCl particles prior to deliquescence and the phase rule, *Aerosol Sci. Technol.*, 42, 281–294, https://doi.org/10.1080/02786820802047115, 2008.
- Wise, M. E., Baustian, K. J., Koop, T., Freedman, M. A., Jensen, E. J., and Tolbert, M. A.: Depositional ice nucleation onto crystalline hydrated NaCl particles: a new mechanism for ice formation in the troposphere, *Atmos. Chem. Phys.*, 12, 1121–1134, https://doi.org/10.5194/acp-12-1121-2012, 2012.
- Wren, S. N., Donaldson, D. J., and Abbatt, J. P. D.: Photochemical chlorine and bromine activation from artificial saline snow, *Atmos. Chem. Phys.*, 13, 9789–9800, https://doi.org/10.5194/acp-13-9789-2013, 2013.
- Yang, X., Neděla, V., Runštuk, J., Ondrušková, G., Krausko, J., Vetráková, L., and Heger, D.: Evaporating brine from frost flowers with electron microscopy and implications for atmospheric chemistry and sea-salt aerosol formation, *Atmos. Chem. Phys.*, 17, 6291–6303, https://doi.org/10.5194/acp-17-6291-2017, 2017.